Graphene Nano-Ribbon Plasmonic Conveyor Belt Network for Optical Trapping and Transportation of Nanoparticles

Peter Qiang Liu*, Puspita Paul

Department of Electrical Engineering, University at Buffalo, The State University of New York, Buffalo, NY 14260, United States

** pqliu@buffalo.edu*

ABSTRACT

Optical tweezers based on metallic plasmonic structures can achieve stable trapping of objects with deep subwavelength dimensions. However, due to the lack of real-time tunability of metallic plasmonic structures, manipulating trapped objects is challenging and usually requires sophisticated tuning of the excitation light source, which limits the application scope of such plasmonic tweezers. Here, we propose the operation principle and analyze the performance of a two-dimensional (2D) network of plasmonic conveyor belts employing electrically tunable graphene plasmonic structures, which can simultaneously and independently trap and transport multiple nanoparticles to arbitrary target locations within the network. Transportation of nanoparticles is achieved by dynamically reconfiguring the carrier density distribution in a graphene nano-ribbon based network structure using an array of back-gates, without a need for any change to the excitation light source. Our numerical analyses show that relatively large optical forces can be induced on nanoparticles with tens of nm characteristic dimensions at a moderate excitation source intensity (e.g. 1 mW/μm^2), and the corresponding trapping potential energy exceeds 10 k_BT at room temperature which guarantees stable trapping during nanoparticle manipulation. Suitable designs of the junction structures in the network are developed, and effective schemes for all-directional routing of nanoparticles at these junctions are proposed and quantitatively analyzed. Such graphene-based plasmonic conveyor belt networks have high design flexibility and system scalability, and therefore may find a wide range of applications in different areas such as lab-on-a-chip, assembling complex nano structures and devices, studying many-body physics and advancing quantum information technologies.

KEYWORDS: graphene, plasmonics, optical tweezers, plasmonic conveyor belt, nanoparticle transportation, mid-infrared

INTRODUCTION

Optical tweezers based on tightly focused laser beams are powerful tools for manipulating mesoscopic objects, including dielectric and metallic particles, cells, bacteria and viruses, and have found a wide range of applications in different areas, particularly in biological and nano science and technologies.[1-8] As the trapping forces of conventional optical tweezers are mainly a result of the optical field gradient near a laser focus, the size of which cannot be arbitrarily small due to the diffraction limit, such optical trapping and manipulation become more challenging for objects with sizes much smaller than the laser wavelength. Nevertheless, conventional optical tweezers can be used to trap deep subwavelength scale objects with resonant optical responses (e.g. plasmonic resonance) or shapes of large aspect ratios (e.g. nanowires, thin flakes).[7,8] Another powerful tool for trapping and manipulating microscopic objects is optoelectronic tweezers,[9,10] which make use of patterned electrodes formed by structured optical illumination on photoconductive materials to induce dielectrophoresis force on target objects. Massive arrays of such optically defined dielectrophoresis traps can be realized and reconfigured in real time. However, as this technique is based on far-field optical image formation, it is also constrained by the diffraction limit and therefore the trap size and density cannot be significantly smaller than the wavelength of light. On the other hand, optically trapping and manipulating nanoscale objects (e.g. dimensions below 100 nm) can be significantly facilitated by confining light beyond the diffraction limit to deep subwavelength scale, which can be achieved using nanophotonic structures such as plasmonic antennas and photonic crystals.[11-13] Optical tweezers based on various plasmonic structures have been theoretically investigated[14-16] and experimentally demonstrated[17-24] in recent years. Stable trapping of nanoparticles with dimensions down to 10 nm and below has been achieved.[21-24]

In addition to stably trapping an object, an ideal optical tweezer should be able to move the trapped object to desired locations. Such a functionality is straightforward to realize for conventional optical tweezers (e.g. by translating the laser beam focus). However, it is significantly more challenging to achieve arbitrary translation of a trapped object using plasmonic tweezers, because the large field gradients are located in the vicinity of the plasmonic structures which have fixed positions, and therefore the objects are usually trapped at these discrete locations. More recently, a "nano-optical conveyor belt" type functionality for transporting nanoparticles along specific directions has been proposed and demonstrated using various designs of plasmonic structures and driving mechanisms.[25-27] This is achieved by employing relatively dense arrays of plasmonic traps in combination with sophisticated tuning of certain properties of the excitation laser beam (e.g. polarization, intensity, frequency), which can cause hopping of a nanoparticle from one plasmonic trap to the next. However, the transported nanoparticle still can only occupy discrete regions centered at the plasmonic traps. Furthermore, the necessity for highly coordinated and precise tuning of the excitation laser beam makes it difficult to manipulate multiple objects simultaneously and independently. This latter limitation is fundamentally due to the lack of real-time tunability of the optical properties of metallic plasmonic structures, and therefore the excitation light source needs to be tuned in order to vary the induced optical forces. On the other hand, tunable plasmonic structures based on various materials with tunable optical properties (e.g. graphene, doped semiconductors and metal oxides) have been demonstrated to operate in various spectral regions.[28-31] Therefore, employing tunable plasmonic materials, such as graphene, is a promising path toward achieving trapping and manipulation of nanoparticles without the need for tuning the excitation light source.

Graphene can be patterned into various types of plasmonic structures such as ribbons,[28,32] disks[33,34] and anti-dots,[35,36] which support widely tunable plasmonic resonances in the mid-infrared to terahertz spectral region, and can facilitate strong light-matter interactions due to the associated large field confinement and enhancement.[37] Optical trapping using different graphene plasmonic structures has been theoretically investigated in several recent work.[38-41] Taking advantage of the exceedingly high field confinement of graphene plasmonic resonances, stable trapping of sub-10 nm nanoparticles can be achieved at moderate

excitation light intensities. As the plasmonic resonance frequency f_p of a graphene structure depend on the graphene carrier density n (and hence its Fermi energy E_F, i.e. $f_p \propto n^{1/4} \propto E_F^{1/2}$), the optical forces exerted on a nanoparticle can be conveniently tuned by changing the graphene carrier density via electrostatic gating, which in turn can achieve relocation of the trapped nanoparticles.[40,41] In this work, we propose the operation principle and analyze the performance of a graphene-based 2D network of plasmonic conveyor belts which can simultaneously and independently trap and transport multiple nanoparticles to arbitrary target locations within this network. Manipulation of nanoparticles are achieved solely by tuning the carrier density (Fermi energy) distribution in the graphene structures using an array of back-gates, without the need for any change to the excitation light source. The presented network system is designed to operate with mid-infrared excitation sources, which can also be rescaled to work with terahertz excitation sources. Therefore, such low photon-energy excitation of the proposed graphene plasmonic conveyor belt networks is also complementary to the visible or near-infrared light sources employed by optical tweezers and metal-based plasmonic tweezers.

RESULTS

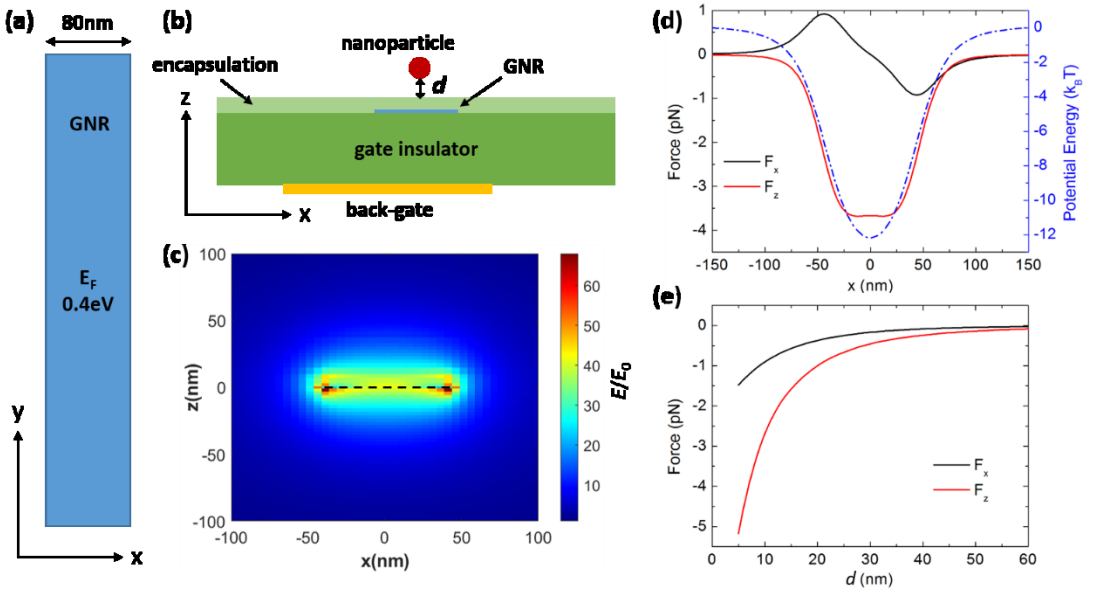

Figure 1. Optical trapping with a uniform GNR structure. (a) Schematic of a GNR with 80 nm ribbon width and the Fermi energy E_F set to 0.4 eV. The GNR is in the x-y plane, and oriented along the y-axis. The GNR is sandwiched between a dielectric substrate and an encapsulation layer as illustrated in (b). (b) Schematic of the cross section of a GNR-based structure for optical trapping of nanoparticles. The GNR is located on a dielectric substrate as well as encapsulated by another 5 nm thick dielectric layer. The graphene carrier density (Fermi energy) can be controlled by a back-gate. (c) Simulated electric near field enhancement profile of the GNR plasmonic resonance, plotted in the x-z plane. The black dashed line represents the GNR along its width direction. (d) Calculated optical forces on a dielectric nanosphere (diameter 50 nm, refractive index 2.5) induced by the GNR plasmonic resonance. The nanosphere is placed at a constant height above the surface of the dielectric encapsulation layer (corresponding to d=10 nm), whereas its x-coordinate is varied from -150 nm to 150 nm. The x-component (F_x) and the z-component (F_z) of optical forces as functions of the nanosphere x-coordinate are plotted in solid lines. The blue dashed line is the corresponding potential energy profile calculated by integrating F_x along the x-axis. (e) Calculated GNR plasmonic resonance-induced optical forces on the same nanosphere as functions of the separation distance d. The x-coordinate of the nanosphere is 40 nm.

As a proof-of-concept demonstration of the unique capability of tunable graphene plasmonics for trapping and manipulating nanoparticles, we focus on graphene nano-ribbon (GNR) structures in this work. GNRs support strong mid-infrared plasmonic resonances and can straightforwardly form networks. The GNR plasmonic resonance can be excited by incident light polarized perpendicular to the GNRs.[28,32] The electromagnetic field associated with this plasmonic resonance is highly confined and enhanced in the vicinity of the GNR and decays exponentially away from the GNR. Therefore, the corresponding large gradient of the near field can exert a significant optical force on nanoparticles located in close proximity to the GNR. Such an optical force is enhanced by several orders of magnitude compared to what can be achieved with a diffraction limited light beam used in conventional optical tweezers.

Optical force induced by a uniform GNR. We first quantitatively discuss the case of a GNR with a uniform Fermi energy distribution. As illustrated in the example in Figure 1a, a uniform GNR with 80 nm width and a Fermi energy E_F=0.4 eV (corresponding to a carrier density of ~10^{13} cm^{-2}) is aligned along the y-axis. We assume that such a GNR is sandwiched between a dielectric substrate and a 5 nm thick encapsulation layer for protecting the GNR from the environment (such as a liquid medium), and the refractive indices of the dielectric substrate and the encapsulation layer are both 1.45, which is similar to those of mid-infrared transparent materials such as CaF_2 and BaF_2. A back-gate below the dielectric substrate is used to control the graphene Fermi energy (see the cross-sectional schematic in Figure 1b). For this system configuration, the GNR plasmonic resonance is at ~9.3 μm with a quality factor of ~10 (see Supporting Information Figure S1), and the corresponding near-field enhancement profile is shown in Fig 1c. The carrier mobility is assumed to be ~16000 cm^2/Vs, which can be readily achieved in high-quality graphene grown by chemical vapor deposition.[42,43] Without loss of generality, in this work we investigate optical forces exerted on spherical dielectric nanoparticles, which are typically more difficult to trap than particles of other shapes,[23] and the refractive index of the environment medium is assumed to be 1. When such a uniform GNR is optically excited at its plasmonic resonance, the optical force on a spherical nanoparticle placed in the vicinity of the GNR (see Figure 1b) can have significant components in both the x-direction and the z-direction, but should be zero in the y-direction as required by symmetry. We simulated the electromagnetic field distributions of the entire system as the dielectric nanosphere was placed at various locations in the vicinity of the GNR, from which we further calculated the GNR induced optical forces on the nanosphere using the Lorentz force density approach (see Methods). In all our simulations, we assumed a normal-incident plane wave excitation source with a moderate intensity of 1 $mW/\mu m^2$. Figure 1d shows the calculated components of the optical force on a nanosphere (diameter 50 nm, refractive index 2.5) positioned at d=10 nm above the encapsulation layer (i.e. 15 nm above the GNR) and at various x-coordinates (the middle line of the GNR corresponds to x=0 nm). Indeed, the optical force has position-dependent components in both the x-direction and the z-direction, but is essentially zero in the y-direction with a numerical noise several orders of magnitude smaller (not plotted). The x-component of the optical force (F_x) tends to localize the nanoparticle to the middle line of the GNR, whereas the z-component (F_z) tends to pull the nanoparticle toward the GNR. Remarkably, the optical force on such a small nanoparticle reaches pN level under the moderate excitation intensity of 1 $mW/\mu m^2$. The corresponding trapping potential energy profile can be calculated by integrating F_x along the x-direction, which is plotted in Figure 1d in the unit of k_BT at room temperature (i.e. temperature T=295 K, k_B is the Boltzmann constant). Clearly, the depth of the potential well exceeds the 10 k_BT requirement for maintaining stable trapping, and the width of the potential well at its half maximum is similar to the width of the GNR (~80 nm). Therefore, the nanoparticle can be stably trapped near the middle line of this uniform GNR, but are free to move along the GNR (i.e. in the y-direction). The optical trapping can be conveniently turned on and off by varying the carrier density of the GNR via changing the back-gate voltage, without making any change to the excitation light source. Since the near-field intensity of the GNR plasmonic resonance decays exponentially as a

function of the distance to the GNR, the optical force on the nanoparticle also decreases rapidly as the nanoparticle is positioned away from the GNR. This can be clearly seen in Figure 1e, which shows the calculated F_x and F_z components of the optical force as a function of the vertical position (d) of the same nanosphere, with its x-coordinate kept at 40 nm (i.e. above the edge of the GNR where F_x approaches its maximum). We also calculated the optical force as a function of the nanosphere diameter, which is plotted in Supporting Information Figure S2. As expected, the optical force (and the trapping potential energy profile) has a strong dependence on the size of the nanoparticle. The trapping force scales slower than the particle volume in the simulated size range, which is mainly due to the fact that the particle diameter in a large portion of this size range is comparable to the evanescent field decay length of the GNR plasmonic resonance, and hence the dipole approximation[7,8] (which leads to the volume scaling law of the optical force) is not accurate for the entire size range. Under the current GNR configuration and material quality assumption, a nanosphere with a diameter of 50 nm and above experience a potential well deeper than 10 k_BT (see Figure 1d). In order to stably trap even smaller objects, we can increase the excitation intensity accordingly and/or improve the graphene carrier mobility.

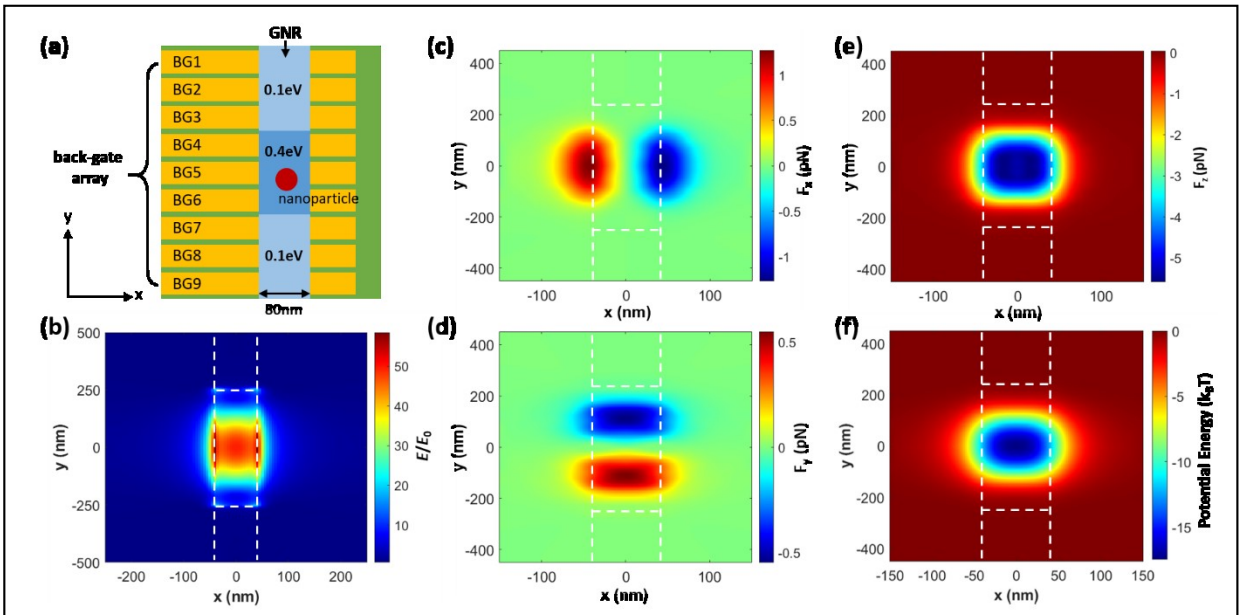

Figure 2. Optical trapping with a non-uniform GNR structure. (a) Schematic of a GNR with a non-uniform Fermi energy (carrier density) distribution along the ribbon length, which can be configured dynamically using a back-gate array as depicted. (b) Simulated electric near field enhancement profile in the x-y plane which is 5 nm above the non-uniform GNR in (a). (c)-(e) Calculated optical force components F_x, F_y and F_z, respectively, induced on the same dielectric nanosphere (diameter 50 nm, refractive index 2.5) placed in the x-y plane corresponding to d=10 nm (i.e. the center of the nanosphere is 40 nm above the non-uniform GNR). (f) Potential energy profile (unit is k_BT) corresponding to the calculated optical force. The white dashed lines in (b)-(f) mark the borders of different GNR sections.

Optical force induced by a non-uniform GNR. The nanoparticle does not experience an optical force in the y-direction due to the translation invariance of the uniform GNR along the y-direction. If this translation invariance is broken, e.g. by varying the graphene carrier density along the GNR, then the plasmonic resonance mode can exhibit localization along the y-direction, and hence the induced optical force can have a significant y-component as well. An example is illustrated in Figure 2a, in which the middle section of

the GNR has $E_F = 0.4$ eV, and the two side sections have a different E_F which can be either lower or higher than that of the middle section. Such a non-uniform Fermi energy distribution can be configured using an array of back-gates as shown in the schematic. As long as the middle section has a length a few times larger than the GNR width, it supports a plasmonic resonance mode at about the same wavelength (~9.3 μm in this case) as that of a uniform GNR with the same Fermi energy (see Supporting Information Figure S1), whereas the two side sections support a plasmonic resonance at a different wavelength. Figure 2b shows the near-field profile of the non-uniform GNR in Figure 2a (the length of the middle section is 500 nm) excited by a normal-incident plane wave at 9.3 μm. Unlike the uniform GNR case, the plasmonic resonance mode of the non-uniform GNR no longer has translation invariance along the y-direction, but is instead spatially confined in the middle section of the GNR. As a result, a nanoparticle above this GNR section experiences an optical force which has not only x- and z-components, but also a y-component that tends to localize the nanoparticle at the center of this resonant GNR section, as shown in Figure 2c-e. The corresponding potential energy profile in the x-y plane is a 2D potential well localized to the resonant GNR section (see Figure 2f). Therefore, the nanoparticle is optically trapped by the plasmonic resonance mode of this non-uniform GNR in all three dimensions. The trapping potential well is also deeper than that of the uniform GNR case, as a result of the additional field confinement and enhancement.

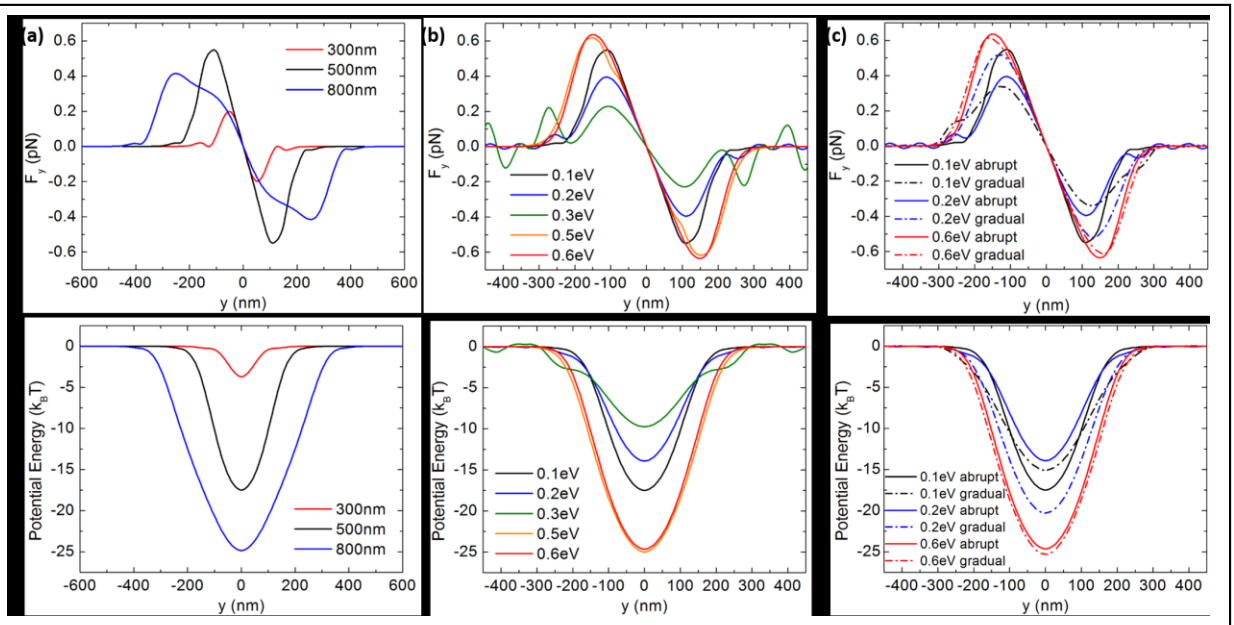

Figure 3. Dependence of optical force and trapping potential on the non-uniform GNR configuration. (a) Upper: The F_y component of optical force on the dielectric nanosphere induced by the plasmonic resonance of a non-uniform GNR, assuming three different GNR resonant section lengths as specified in the legend. Lower: The corresponding potential energy profiles. (b) Upper: The F_y component of optical force on the dielectric nanosphere induced by the plasmonic resonance of a non-uniform GNR, assuming different Fermi energies of the non-resonant side sections as specified in the legend. The middle resonant section has a length of 500 nm and E_F=0.4 eV. Lower: The corresponding potential energy profiles. (c) Upper: The F_y component of optical force on the dielectric nanosphere induced by the plasmonic resonance of a non-uniform GNR, assuming either abrupt or gradual Fermi energy transitions for various Fermi energies of the non-resonant side sections. Lower: The corresponding potential energy profiles. The nanosphere (diameter 50 nm, refractive index 2.5) is placed at a constant height (d=10 nm), and moved in the y-direction along the middle line of GNR for all the calculations shown in this figure.

Clearly, the length of the resonant GNR section is a critical parameter which determines the plasmonic resonance mode and hence the optical force and trapping potential profile. Figure 3a shows the calculated y-component of the optical forces (F_y, upper panel) and the corresponding potential energy profiles (lower panel), as the y-coordinate of the nanoparticle varies along the middle line of the GNR. Calculations based on three different resonant section lengths are compared in Figure 3a, with the Fermi energy of the side sections set to 0.1 eV. It can be seen that when the resonant section is relatively short (e.g. ~300 nm), the optical force and the potential well depth both decrease significantly, which may not achieve stable trapping. When the resonant section is relatively long (e.g. ~800 nm), the trapping potential well is much deeper, but its width in the y-direction also increases significantly. The intermediate case with 500 nm resonant section length leads to the largest F_y, and corresponds to the best trade-off between trapping stability and spatial confinement in the y-direction. Therefore, most of the results described in the following are based on GNR structures with 500 nm resonant section length.

The distribution of Fermi energy in different sections is another important factor for determining the trapping performance. For a given GNR width, E_F of the resonant section is always set to the value which matches the plasmonic resonance to the excitation wavelength. Then a sufficient Fermi energy contrast between the resonant section and the two side sections needs to be established, so that the plasmonic resonance mode and hence the trapping potential well are localized to the resonant section. Figure 3b shows the calculated F_y (upper panel) and the corresponding potential energy profile (lower panel) for various E_F values of the side sections, ranging from 0.1 eV to 0.6 eV, as functions of the nanosphere y-coordinate. This comparison shows that in general larger Fermi energy contrast (either positive or negative) leads to larger optical force and deeper trapping potential well. Nevertheless, even a moderate Fermi energy contrast (e.g. 0.1 eV) is sufficient to achieve the potential well depth required for stable trapping (~10 k_BT). Furthermore, our calculation reveals that when the side sections have a higher Fermi energy than the resonant section in the middle (i.e. a negative Fermi energy contrast), the trapping force and the potential well depth are considerably larger than when the side sections have a lower Fermi energy (i.e. a positive Fermi energy contrast). Therefore, establishing a higher Fermi energy in the side sections allow for a reduction of the excitation source intensity, although this also requires applying a significantly larger gate voltage which can be challenging in practice.

The results discussed so far are obtained under the assumption that the Fermi energy transitions between the different sections are abrupt. In reality, such a transition should occur gradually within a finite region, the length of which depends on the details of the gates, such as the gate insulator thickness and the separation between neighboring gate electrodes. Therefore, we also investigated the optical forces and trapping potential profiles of such non-uniform GNR structures with gradual Fermi energy transition regions. A comparison between these two different scenarios is presented in Figure 3c. The gradual transition regions are all assumed to be 40 nm in length regardless of the Fermi energy contrast, and the Fermi energy varies linearly in the transition regions. It can be seen that both the optical force and the potential well profiles associated with the gradual transition scenario are not significantly different from those of the abrupt transition scenario. On one hand, the gradual transition regions make the resonant section effectively longer, which tends to increase the trapping potential depth. On the other hand, the gradual transition regions lower the Fermi energy contrast, which tends to decrease the trapping potential depth. These two competing factors can lead to either a moderate increase (e.g. side section E_F=0.2 eV) or a moderate decrease (e.g. side section E_F=0.1 eV) of the trapping force and potential depth, depending on the specific Fermi energy configuration. Although the gradual Fermi energy transition in a real structure can have a more complex profile than the linear transition assumed here, based on the results in Figure 3c, we do not expect such specific details to have a significant impact on the trapping force and potential energy profiles. Overall, the abrupt transition assumption can be considered a simple yet relatively accurate first-order approximation to the gradual transition scenario.

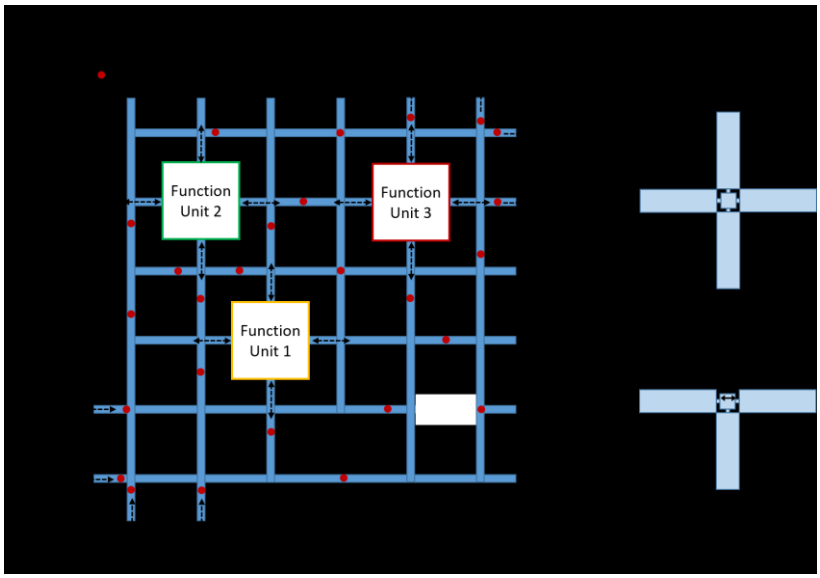

Figure 4. GNR plasmonic conveyor belt network. (a) Conceptual schematic illustrating the proposed GNR plasmonic conveyor belt network which can simultaneously and independently trap and transport multiple nanoparticles to different target locations within the network. (b) Schematics of the cross junction and tee junction of the GNR network with geometric details of the structure designs.

GNR plasmonic conveyor belt network structure and operation. In addition to the capability of stably trapping nanoparticles, another key advantage of the proposed non-uniform GNR structure is that it can function as a conveyor belt to transport the trapped nanoparticles along the GNR. This is straightforwardly achieved by dynamically reconfiguring the Fermi energy distribution in the GNR using the back-gate array, which shifts the position of the trapping potential well along the GNR. In stark contrast to the previously demonstrated nano-optical conveyor belts based on metallic plasmonic structures,[25-27] such a GNR plasmonic conveyor belt does not need any change to the excitation light source. Furthermore, the trapped objects can be transported to any target location along the GNR, with a position resolution equal to half of the gate array pitch, which can reach ~10 nm range using standard nanofabrication technology such as electron beam lithography. Therefore, such GNR-based plasmonic conveyor belts are a potentially more convenient, reliable and versatile solution than the metal-based plasmonic conveyor belts. More importantly, we can further extend this 1D structure to form a 2D network of GNR plasmonic conveyor belts, as conceptually depicted in Figure 4a. Such a 2D network can have multiple input and output ports, as well as embedded units with various functionalities. Multiple nanoparticles can be simultaneously and independently trapped and transported between different ports and embedded function units within the network, all controlled electrically by a 2D back-gate array. Such a conveyor belt network for nanoscale objects may find a variety of applications, ranging from lab-on-a-chip for biochemical assays to studying many-body physics and advancing quantum information technologies.

In addition to straight GNRs, the proposed 2D GNR network also consists of another two key components, i.e., cross junctions and tee junctions, as shown in Figure 4b. A fully functioning 2D conveyor belt network requires that trapped nanoparticles can be routed at will at these junctions. In the following, we describe in details suitable operation schemes for routing trapped objects at these two types of junctions, which are

relatively intuitive and similar to that for transporting trapped objects along GNRs. To excite plasmonic resonances in both horizontal and vertical GNRs, either an unpolarized laser beam or a superposition of two orthogonal linearly-polarized laser beams can be used. It can be clearly seen in Figure 4b that the structures of the cross junction and the tee junction are not simply formed by intersecting two orthogonal GNRs. Instead, these junctions consist of a slightly smaller graphene square (side length 55 nm) connected to the 80 nm wide GNRs via narrower graphene strips (15 nm wide). We designed such junction structures because they support localized plasmonic resonances which tend to trap nanoparticles at the junction center, and hence it is more straightforward to achieve all-directional routing at such junctions. A junction formed by simply intersecting two orthogonal GNRs can only trap nanoparticles adjacent to the junction center, which is a result of its plasmonic resonance mode profile and not ideal for all-directional routing.

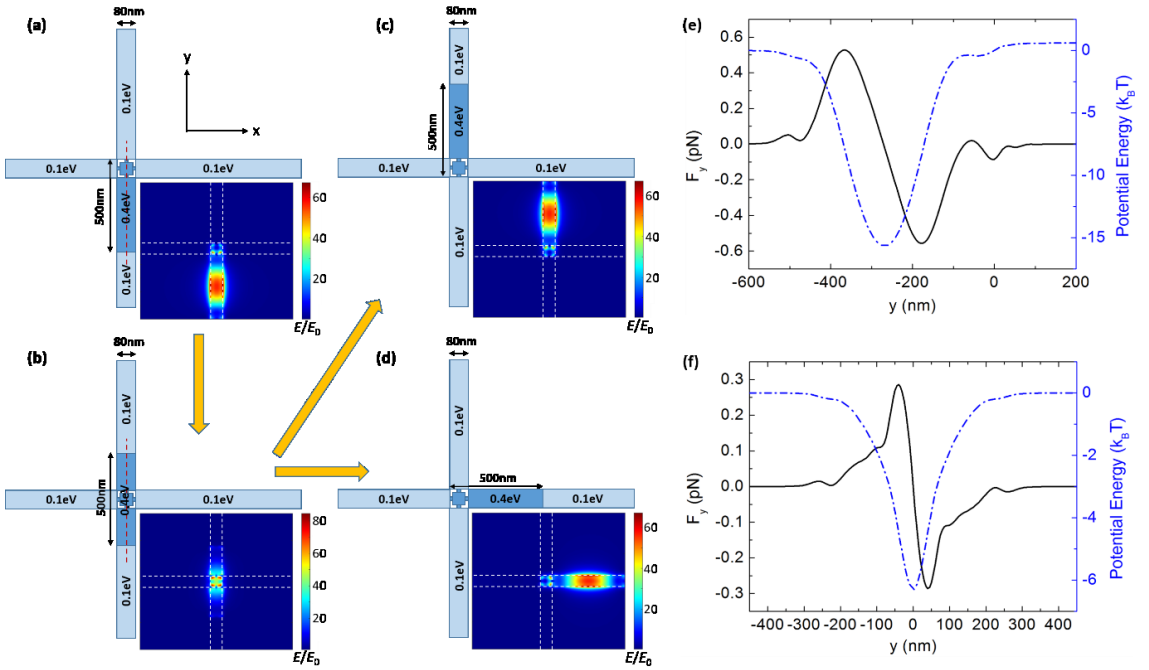

Figure 5. All-directional routing at the cross junction. (a)-(d) Schematics showing the Fermi energy configurations of the cross junction and the corresponding near-field profiles (insets) associated with the key steps for routing a nanoparticle. In each configuration, the nanoparticle is trapped at the high-field region, which can be seen from the optical force and potential energy profile calculations in (e) and (f). A gradual transition from one configuration to another configuration (as indicated by the arrows) transports the trapped nanoparticle from one trapping position to the other. (e) The calculated optical force on the nanosphere and the corresponding potential energy profile for the configuration in (a) (and in (c) or (d) when applying a mirror image operation or a 90° rotation operation, respectively). The optical force is calculated as the nanosphere coordinate varies along the red dashed line in (a). (f) The calculated optical force on the nanosphere and the corresponding potential energy profile for the configuration in (b). The optical force is calculated as the nanosphere coordinate varies along the red dashed line in (b). The nanosphere is kept at a constant height corresponding to d=10 nm for all the calculations.

All-directional routing at a cross junction. A suitable scheme for dynamically reconfiguring the Fermi energy distribution for all-directional routing at a cross junction is shown in Figure 5. The schematics in Figure 5a-d show the Fermi energy configurations of such a cross junction in several representative steps of the routing procedure, with the insets showing the near-field profiles of the corresponding plasmonic resonance mode. For instance, we can assume the same dielectric nanosphere enters from the lower GNR branch of the cross junction and needs to be routed to one of the other three GNR branches. The first step is to transport the nanoparticle along the lower GNR branch toward the cross junction. This is achieved by gradually shifting the resonant GNR section (500 nm long, E_F=0.4 eV) along the positive y-direction, until this 500 nm long section includes the graphene square at the junction center, which corresponds to the schematic in Figure 5a. In this case, the nanoparticle is trapped at the location with the highest field intensity in the lower GNR branch. The second step is to further shift this resonant GNR section along the positive y-direction until its middle point is at the junction center, which corresponds to a transition from Figure 5a to Figure 5b. The highest field intensity of the configuration in Figure 5b is localized at the graphene square, as shown in the inset. Therefore, the nanoparticle is now trapped exactly at the junction center. To subsequently route the nanoparticle from the junction center to any GNR branch, we simply need to gradually shift the resonant section into that GNR branch as the final step. For example, a gradual transition from Figure 5b to Figure 5c or Figure 5d corresponds to routing the nanoparticle into the upper or the right GNR branch, respectively. Essentially, during the entire routing process, the nanoparticle is always localized near the center of the resonant GNR section and moves along with this section from one branch to another. This intuitive routing scheme is supported by our quantitative calculation of the optical forces and the corresponding potential energy profiles for the different Fermi energy configurations. Figure 5e shows the F_y component of optical force and the corresponding potential energy profile as a function of the y-coordinate of the dielectric nanosphere, assuming the Fermi energy configuration in Figure 5a. Indeed, the optical force tends to trap the nanoparticle at the location with the highest near-field intensity in the lower GNR branch, and the depth of the trapping potential well exceeds 10 k_BT needed for stable trapping. Due to the 4-fold rotation symmetry of the cross junction, the calculated results in Figure 5e also applies to the configurations in Figure 5c and Figure 5d after making the corresponding symmetry operations. Figure 5f shows the F_y component of optical force and the corresponding potential energy profile as a function of the y-coordinate of the dielectric nanosphere, assuming the Fermi energy configuration in Figure 5b. In this case, the optical force (the potential well) tends to localize the nanoparticle exactly at the cross junction center. However, the optical force and the potential well depth are smaller than those in Figure 5e, which is mainly due to the fact that the plasmonic resonance mode for this configuration has a relatively smaller high-intensity region (see Figure 5b). This may not be an issue if the nanoparticle only needs to be trapped at the junction center for a short period of time. On the other hand, this potential well depth can be increased to ~10 k_BT by moderately increasing the excitation source intensity to ~1.5 mW/μm^2.

All-directional routing at a tee junction. Routing nanoparticles at a tee junction can be accomplished using a similar scheme, which is depicted in Figure 6. Again, we assume the nanoparticle enters from the lower GNR branch of the tee junction. A gradual transition from the configuration in Figure 6a to that in Figure 6b moves the trapped nanoparticle from the lower GNR branch to the center of the tee junction (i.e. the graphene square). A subsequent transition from Figure 6b to Figure 6c moves the nanoparticle straight across the junction into the upper GNR branch, whereas a gradual transition from Figure 6b to Figure 6d moves the nanoparticle into the horizontal GNR branch on the right side, accomplishing a 90° turn at the tee junction. The time reversal of these processes are also applicable, and therefore a nanoparticle entering from the horizontal branch or the upper branch can also be routed to any other branch via the tee junction. The validity of this all-directional routing scheme for the tee junction is also supported by our calculation of the optical forces and the potential energy profiles. Figures 6e-g show the optical forces and the potential energy profiles corresponding to the configurations in Figure 6a, Figure 6b, and Figure 6d, respectively. Again, for all the calculations, the coordinate of the dielectric nanosphere is varied in the direction parallel

to the resonant GNR section. As expected, in each configuration the center of the trapping potential well matches the location with the highest near field (see insets of Figure 6a-d). The nanoparticle is trapped in and follows the movement of the potential well to complete various routing paths, as the Fermi energy distribution at the tee junction is dynamically reconfigured. These results are also quantitatively similar to those of the cross junction in Figure 5.

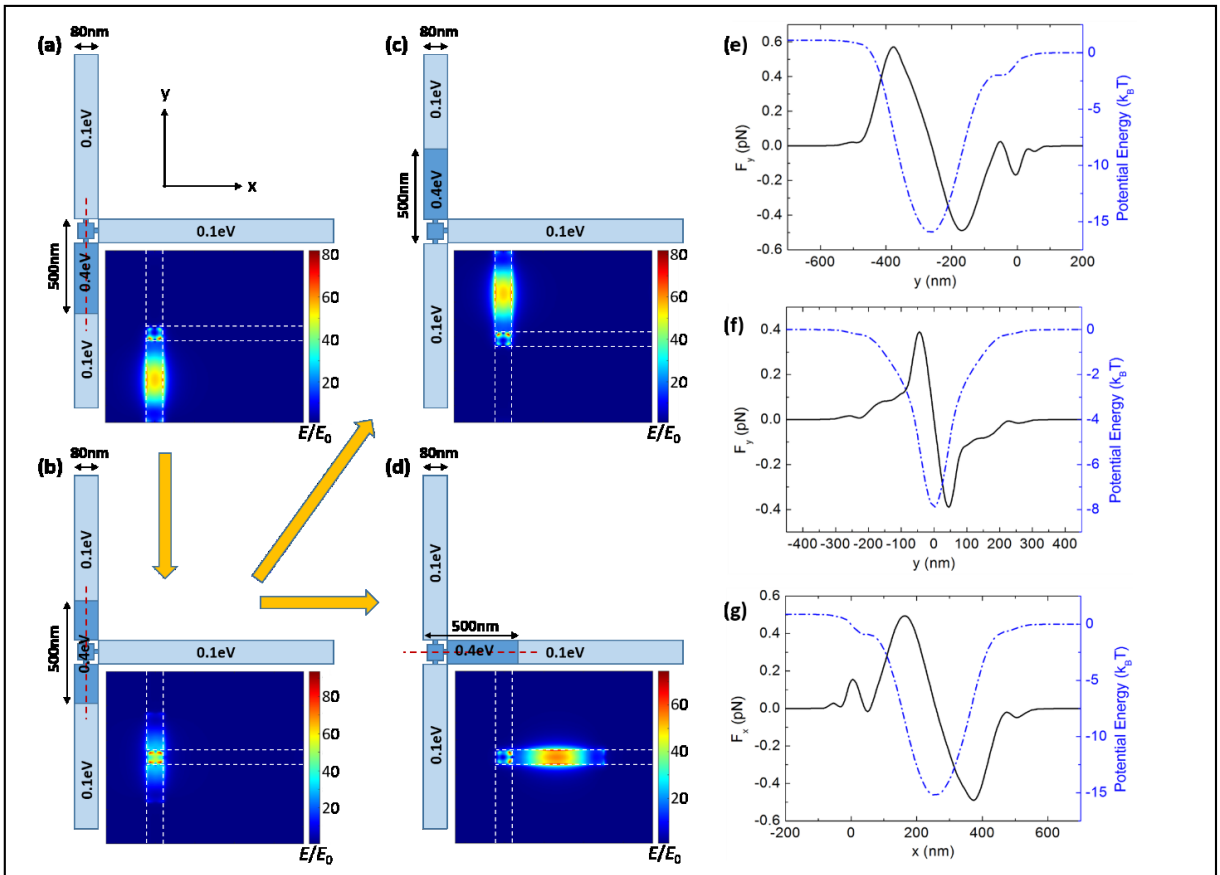

Figure 6. All-directional routing at the tee junction. (a)-(d) Schematics showing the Fermi energy configurations of the tee junction and the corresponding near-field profiles (insets) associated with the key steps for routing a nanoparticle. In each configuration, the nanoparticle is trapped at the high-field region, which can be seen from the optical force and potential energy profile calculations in (e)-(g). A gradual transition from one configuration to another configuration (as indicated by the arrows) transports the trapped nanoparticle from one trapping position to the other. (e) The calculated optical force on the nanosphere and the corresponding potential energy profile for the configuration in (a) (or in (c) when applying a mirror symmetry operation). (f) The calculated optical force on the nanosphere and the corresponding potential energy profile for the configuration in (b). (g) The calculated optical force on the nanosphere and the corresponding potential energy profile for the configuration in (d). The optical forces are calculated as the nanosphere coordinate varies along the red dashed line in each configuration schematic. The nanosphere is kept at a constant height corresponding to d=10 nm for all the calculations.

DISCUSSION

We have proposed and analyzed the performance of a plasmonic conveyor belt network based on GNRs which can simultaneously and independently trap and transport multiple nanoparticles to different target locations within the 2D network. Our quantitative analyses of the optical forces and the corresponding potential energy profiles are based on local regions of the proposed network (either a linear GNR section or a junction) containing a single nanoparticle. Nevertheless, since a plasmonic resonance mode is determined by the local GNR geometry and Fermi energy distribution, and the mode is also localized to the resonant GNR section, it is hardly influenced by a noncontiguous region of the network. Therefore, different regions of such a 2D GNR network can perform trapping, transportation and routing of different nanoparticles simultaneously and independently. Essentially, each GNR section between two neighboring junctions (see Figure 4) can be considered as an independent plasmonic conveyor belt for manipulating one nanoparticle. Different nanoparticles in different GNR branches can be routed at the same junction following an appropriate sequence, the details of which depend on the specific application and need.

We have presented suitable designs for the cross junctions and the tee junctions, which are crucial components of the proposed 2D conveyor belt network. These junction designs enable simple and intuitive schemes for reconfiguring the Fermi energy distribution to achieve all-directional routing. This is mainly because their plasmonic resonance modes trap the nanoparticle exactly at the junction center, which should be a crucial goal when making alternative designs for such junctions. We expect that the junction designs can be further optimized by changing the sizes and/or the shapes, so that the trapping potential depth can be further increased. The results presented in this work are mostly based on a spherical dielectric nanoparticle with 50 nm diameter. If for example the diameter of the nanosphere is 20 nm, the trapping potential energy (~2 k_BT) is about 1/6 of that for the nanosphere with 50 nm diameter, as shown in the Supporting Information Figure S3. However, we expect stable trapping and manipulation of such small dielectric objects (dimensions of about 20 nm or below) can be achieved with design optimizations in various aspects, such as increasing the graphene carrier density, decreasing the GNR width and the operating wavelength, which should lead to larger field gradients of the plasmonic resonance mode. Alternative designs of graphene plasmonic structures and graphene-metal hybrid structures[44] can also be explored to enhance the optical forces on smaller objects. Moreover, as the plasmonic response of a graphene structure is highly sensitive to its environment, the self-induced back-action effect can be exploited to further increase the trapping and manipulation performance.

The fact that graphene plasmonic structures enable the use of mid-infrared or even terahertz excitation sources for optical trapping and manipulation can be a key advantage for certain applications, since such relatively low photon energy is less likely to cause undesired light-induced changes to the trapped objects (e.g. photoionization or photobleaching). Furthermore, as vibrational modes in molecules and optical phonons in crystalline materials are mostly in the mid-infrared to terahertz spectral region, optical trapping and manipulation using mid-infrared or terahertz sources can also be combined with various infrared spectroscopy techniques for characterizing these material excitations in the trapped objects. Although the excitation wavelengths in this spectral region are much larger than those of near-infrared or visible sources used in metal-based plasmonic tweezers, the GNRs can still induce significant optical forces on nanoparticles at a moderate excitation intensity, thanks to the exceedingly large field confinement and enhancement of graphene surface plasmons. In addition, the optical force and trapping potential energy can be significantly enhanced by exploiting the resonantly enhanced polarizability due to molecular vibrations and/or optical phonons in target objects.

Another important issue for plasmonic tweezers in general is the heating due to light absorption in the resonant plasmonic structures. A comprehensive and quantitative investigation of the heat generation and dissipation aspects of the proposed structures is beyond the scope of this work. Nevertheless, we point out

that graphene has remarkably large thermal conductivity, which facilitates spreading and dissipation of heat generated at the localized resonant sections in a network structure. A variety of candidate materials with both high thermal conductivity and transparency windows in the mid-infrared region, such as diamond, silicon carbide and aluminum nitride, can be used as the substrate to further mitigate any potential heating effect. On the other hand, although heating can cause undesirable issues, it can also be utilized to assist optical trapping and manipulation by implementing suitable structure designs and/or combining with additional physical effects, as has been demonstrated previously.[45]

The proposed GNR plasmonic conveyor belt network have high design flexibility and system scalability. As the GNRs are protected by a thin encapsulation layer in this proof-of-concept design, the system can operate in various liquid media and be integrated with other types of structures and devices. Therefore, it may find a wide range of applications in different areas, such as lab-on-a-chip for biochemical assays, assembling nanoparticles to form more complex structures and devices, as well as manipulating nanoparticles for studying many-body physics and advancing quantum information technologies. Our work provide physical insights and design guidance for further experimental demonstration and development of such a potentially versatile technology.

METHODS

Simulation of electromagnetic field distributions and calculation of optical forces. The electromagnetic field distributions of the investigated systems were simulated using Lumerical FDTD which is based on the finite difference time domain method. Graphene was modeled as a 2D surface with an optical conductivity expression based on the Kubo formula.[46] The carrier scattering rate of graphene was set to 1 meV in terms of energy (corresponding to a scattering time of ~0.66 ps and a carrier mobility of ~16000 cm^2/Vs). Periodic boundary conditions were used for the x and y boundaries with the periods set to be 1 μm in both directions, which were large enough so that the plasmonic resonance modes were determined by the local structure rather than by the periodicity. A broadband normal-incident plane wave with a center wavelength at ~9.3 μm was used as the excitation source. The calculation of optical forces on the target object (i.e. the dielectric nanosphere) was based on taking the volumetric integral of the Lorentz force density[47] over a cubic volume which completely contained the dielectric nanosphere but no other object. We chose this method after we compared it with the Maxwell stress tensor method, and found that the former had less numerical noise than the latter for calculating forces on such nano-scale objects.

ASSOCIATED CONTENT

The Supporting Information is available free of charge via the internet at http://pubs.acs.org.

Transmission spectra of GNR arrays; optical force dependence on trapped nanoparticle size; optical force and trapping potential energy of a dielectric nanosphere with 20 nm diameter

AUTHOR INFORMATION

Corresponding Author

Peter Qiang Liu, Email: pqliu@buffalo.edu

Author Contributions

P.Q.L. conceived the idea. P.Q.L. and P.P. performed the simulation and calculation. P.Q.L. wrote the manuscript with input from P.P.

The authors declare no competing interests.

ACKNOWLEDGEMENT

This work is supported in part by the National Science Foundation (NSF) (Award No. ECCS-1847203).

REFERENCES

(1) Ashkin, A.; Dziedzic, J. M.; Bjorkholm, J. E.; Chu, S. Observation of a single-beam gradient force optical trap for dielectric particles. *Opt. Lett.* **1986**, *11*, 288-290.

(2) Molloy, J. E.; Padgett, M. J. Lights, action: optical tweezers. *Cont. Phys.* **2002**, *43*, 241-258.

(3) Neuman, K. C.; Block, S. M. Optical trapping. *Rev. Sci. Instrum.* **2004**, *75*, 2784-2809.

(4) Bustamante, C.; Bryant, Z.; Smith, S. B. Ten years of tension: single-molecule DNA mechanics. *Nature* **2003**, *421*, 423-427.

(5) MacDonald, M. P.; Spalding, G. C.; Dholakia, K. Microfluidic sorting in an optical lattice. *Nature* **2003**, *426*, 421-424.

(6) Abbondanzieri, E. A.; Greenleaf, W. J.; Shaevitz, J. W.; Landick, R.; Block, S. M. Direct observation of base-pair stepping by RNA polymerase. *Nature* **2005**, *438*, 460-465.

(7) Marago, O. M.; Jones, P. H.; Gucciardi, P. G.; Volpe, G.; Ferrari, A. Optical trapping and manipulation of nanostructures. *Nat. Nanotechnol.* **2013**, *8*, 807-819.

(8) Spesyvtseva, S. E. S.; Dholakia, K. Trapping in a material world. *ACS Photonics* **2016**, *3*, 719-736.

(9) Chiou, P. Y.; Ohta, A. T.; Wu, M. C. Massively parallel manipulation of single cells and microparticles using optical images. *Nature* **2005**, *436*, 370-372.

(10) Jamshidi, A.; Pauzauskie, P. J.; Schuck, P. J.; Ohta, A. T.; Chiou, P.-Y. Chou, J.; Yang, P.; Wu, M. C. Dynamic manipulation and separation of individual semiconducting and metallic nanowires. *Nat. Photonics* **2008**, *2*, 85-89.

(11) Juan, M. L.; Righini, M.; Quidant, R. Plasmon nano-optical tweezers. *Nat. Photonics* **2011**, *5*, 349-356.

(12) Mandal, S.; Serey, X.; Erickson, D. Nanomanipulation using silicon photonic crystal resonators. *Nano Lett.* **2010**, *10*, 99-104.

(13) Xu, Z.; Song, W.; Crozier, K. B. Optical trapping of nanoparticles using all-silicon nanoantennas. *ACS Photonics* **2018**, *5*, 4993-5001.

(14) Novotny, L.; Bian, R. X.; Xie, X. S. Theory of nanometric optical tweezers. *Phys. Rev. Lett.* **1997**, *79*, 645-648.

(15) Martin, O. J. F.; Girard, C. Controlling and tuning strong optical field gradients at a local probe microscope tip apex. *Appl. Phys. Lett.* **1997**, *70*, 705-707.

(16) Okamoto, K.; Kawata, S. Radiation force exerted on subwavelength particles near a nanoaperture. *Phys. Rev. Lett.* **1999**, *83*, 4534-4537.

(17) Volpe, G.; Quidant, R.; Badenes, G.; Petrov, D. Surface plasmon radiation forces. *Phys. Rev. Lett.* **2006**, *96*, 238101.

(18) Righini, M.; Zelenina, A. S.; Girard, C.; Quidant, R. Parallel and selective trapping in a patterned plasmonic landscape. *Nat. Phys.* **2007**, *3*, 477-480.

(19) Grigorenko, A. N.; Roberts, N. W.; Dickinson, M. R.; Zhang, Y. Nanometric optical tweezers based on nanostructured substrates. *Nat. Photonics* **2008**, *2*, 365-370.

(20) Juan, M. L.; Gordon, R.; Pang, Y.; Eftekhari, F.; Quidant, R. Self-induced back-action optical trapping of dielectric nanoparticles. *Nat. Phys.* **2009**, *5*, 915-919.

(21) Zhang, W.; Huang, L.; Santschi, C.; Martin, O. J. F. Trapping and sensing 10 nm metal nanoparticles using plasmonic dipole antennas. *Nano Lett.* **2010**, *10*, 1006-1011.

(22) Tsuboi, Y.; Shoji, T.; Kitamura, N.; Takase, M.; Murakoshi, K.; Mizumoto, Y.; Ishihara, H. Optical trapping of quantum dots based on gap-mode-excitation of localized surface plasmon. *J. Phys. Chem. Lett.* **2010**, *1*, 2327-2333.

(23) Pang, Y.; Gordon, R. Optical trapping of 12 nm dielectric spheres using double-nanoholes in a gold film. *Nano Lett.* **2011**, *11*, 3763-3767.

(24) Pang, Y.; Gordon, R. Optical trapping of a single protein. *Nano Lett.* **2012**, *12*, 402-406.

(25) Hansen, P.; Zheng, Y.; Ryan, J.; Hesselink, L. Nano-optical conveyor belt, part I: theory. *Nano Lett.* **2014**, *14*, 2965-2970.

(26) Zheng, Y.; Ryan, J.; Hansen, P.; Cheng, Y.-T.; Lu, T.-J.; Hesselink, L. Nano-optical conveyor belt, part II: demonstration of handoff between near-field optical traps. *Nano Lett.* **2014**, *14*, 2971-2976.

(27) Kang, Z.; Lu, H.; Chen, J.; Chen, K.; Xu, F.; Ho, H.-P. Plasmonic graded nano-disks as nano-optical conveyor belt. *Opt. Express* **2014**, *22*, 19567-19572.

(28) Ju, L.; Geng, B.; Horng, J.; Girit, C.; Martin, M.; Hao, Z.; Bechtel, H. A.; Liang, X.; Zettl, A.; Shen, Y. R.; Wang, F. Graphene plasmonics for tunable terahertz metamaterials. *Nat. Nanotechnol.* **2011**, *6*, 630-634.

(29) Wagner, M.; MeLeod, A. S.; Maddox, S. J.; Fei, Z.; Liu, M.; Averitt, R. D.; Fogler, M. M.; Bank, S. R.; Keilmann, F.; Basov, D. N. Ultrafast dynamics of surface plasmons in InAs by time-resolved infrared nanospectroscopy. *Nano Lett.* **2014**, *14*, 4529-4534.

(30) Kinsey, N.; DeVault, C.; Kim, J.; Shalaev, V. M.; Boltasseva, A. Epsilon-near-zero Al-doped ZnO for ultrafast switching at telecom wavelengths. *Optica* **2015**, *2*, 616-622.

(31) Yang, Y.; Kelley, K.; Sachet, E.; Campione, S.; Luk, T. S.; Maria, J.-P.; Sinclair, M. B.; Brener, I. Femtosecond optical polarization switching using a cadmium oxide-based perfect absorber. *Nat. Photonics* **2017**, *11*, 390-395.

(32) Brar, V. W.; Jang, M. S.; Sherrott, M.; Lopez, J. J.; Atwater, H. A. Highly confined tunable mid-infrared plasmonics in graphene nanoresonators. *Nano Lett.* **2013**, *13*, 2541-2547.

(33) Yan, H.; Li, X.; Chandra, B.; Tulevski, G.; Wu, Y.; Freitag, M.; Zhu, W.; Avouris, P.; Xia, F. Tunable infrared plasmonic devices using graphene/insulator stacks. *Nat. Nanotechnol.* **2012**, *7*, 330-334.

(34) Fang, Z.; Wang, Y.; Schlather, A. E.; Liu, Z.; Ajayan, P. M.; Garcia de Abajo, F. J.; Nordlander, P.; Zhu, X.; Halas, N. J. Active tunable absorption enhancement with graphene nanodisk arrays. *Nano Lett.* **2014**, ***14***, 299-304.

(35) Zhu, X.; Wang, W.; Yan, W.; Larsen, M. B.; Boggild, P.; Pedersen, T. G.; Xiao, S.; Zi, J.; Mortensen N. A. Plasmon-phonon coupling in large-area graphene dot and antidot arrays fabricated by nanosphere lithography. *Nano Lett.* **2014**, *14*, 2907-2913.

(36) Liu, P. Q.; Valmorra, F.; Maissen, C.; Faist, J. Electrically tunable graphene anti-dot array terahertz plasmonic crystals exhibiting multi-band resonances. *Optica* **2015**, *2*, 135-140.

(37) Koppens, F. H.; Chang, D. E.; Garcia de Abajo, F. J. Graphene plasmonics: a platform for strong light-matter interactions. *Nano Lett.* **2011**, *11*, 3370-3377.

(38) Zhu, B.; Ren, G.; Gao, Y.; Yang, Y.; Cryan, M. J.; Jian, S. Giant gradient force for nanoparticle trapping in coupled graphene strips. *IEEE Photon. Technol. Lett.* **2015**, *27*, 891-894.

(39) Zhang, J.; Liu, W.; Zhu, Z.; Yuan, X.; Qin, S. Towards nano-optical tweezers with graphene plasmons: numerical investigation of trapping 10-nm particles with mid-infrared light. *Sci. Rep.* **2016**, *6*, 38086.

(40) Abbasi, M. M.; Darbari, S.; Moravvej-Farshi, M. K. Tunable plasmonic force switch based on graphene nano-ring resonator for nanomanipulation. *Opt. Express* **2019**, *27*, 26648-26660.

(41) Danesh, M.; Zadeh, M. J.; Zhang, T.; Zhang, X.; Gu, B.; Lu, J.-S.; Cao, T.; Liu, Z.; Wee, A. T. S.; Qiu, M.; Bao, Q.; Maier, S.; Qiu, C.-W. Monolayer conveyor for stably trapping and transporting sub-1 nm particles. *Laser Photonics Rev.* **2020**, *14*, 2000030.

(42) Hao, Y.; Bharathi, M. S.; Wang, L.; Liu, Y.; Chen, H.; Nie, S.; Wang, X.; Chou, H.; Tan, C.; Fallahazad, B.; Ramanarayan, H.; Magnuson, C. W.; Tutuc, E.; Yakobson, B. I.; McCarty, K. F.; Zhang, Y.-W.; Kim, P.; Hone, J.; Colombo, L.; Ruoff, R. S. The role of surface oxygen in the growth of large single-crystal graphene on copper. *Science* **2013**, *342*, 720-723.

(43) Banszerus, L.; Schmitz, M.; Engels, S.; Dauber, J.; Oellers, M.; Haupt, F.; Watanabe, K.; Taniguchi, T.; Beschoten, B.; Stampfer, C. Ultrahigh-mobility graphene devices from chemical vapor deposition on reusable copper. *Sci. Adv.* **2015**, *1*, e1500222.

(44) Miao, X.; Li, G.; Xiao, L.; Liu, P. Q. Graphene antidote terahertz plasmonic metasurfaces employing self-aligned metal cores for sensing applications. *ACS Appl. Nano Mater.* **2019**, *2*, 6798-6803.

(45) Ndukaife, J. C.; Kildishev, A. V.; Nnanna, A. G. A.; Shalaev, V. M.; Wereley, S. T.; Boltasseva, A. Long-range and rapid transport of individual nano-objects by a hybrid electrothermoplasmonic nanotweezer. *Nat. Nanotechnol.* **2015**, *11*, 53-59.

(46) Hanson, G. W. Dyadic Green's functions and guided surface waves for a surface conductivity model of graphene. *J. Appl. Phys.* **2008**, *103*, 064302.

(47) Novotny, L.; Hecht, B. *Principles of Nano-Optics*, 2nd edition, Cambridge University Press: Cambridge, **2012**, 448-453.

For Table of Contents Use Only

Graphene Nano-Ribbon Plasmonic Conveyor Belt Network for Optical Trapping and Transportation of Nanoparticles

Peter Qiang Liu*, Puspita Paul

Brief synopsis: the TOC graph shows a schematic of the proposed graphene nano-ribbon plasmonic conveyor belt network architecture, a schematic of the detailed device structure, and a simulated trapping potential energy profile for a dielectric nanosphere.